Int J Fract (2017) 208:97–113
https://doi.org/10.1007/s10704-017-0217-z

IUTAM BALTIMORE

Numerical investigation of statistical variation of concrete damage properties between scales

Shixue Liang · Jiun-Shyan Chen · Jie Li · Shih-Po Lin · Sheng-Wei Chi · Michael Hillman · Michael Roth · William Heard

Received: 7 January 2017 / Accepted: 4 May 2017 / Published online: 7 June 2017

Abstract Concrete is typically treated as a homogeneous material at the continuum scale. However, the randomness in micro-structures has profound influence on its mechanical behavior. In this work, the relationship of the statistical variation of macro-scale concrete properties and micro-scale statistical variations is investigated. Micro-structures from CT scans are used to quantify the stochastic properties of a high strength concrete at the micro-scale. Crack propagation is then simulated in representative micro-structures subjected to tensile and shear tractions, and damage evolution functions in the homogenized continuum are extracted using a Helmholtz free energy correlation. A generalized density evolution equation is employed to represent the statistical variations in the concrete micro-structures as well as in the associated damage evolution functions of the continuum. This study quantifies how the statistical variations in void size and distribution in the concrete microstructure affect the statistical variation of material parameters representing tensile and shear damage evolutions at the continuum scale. The simulation results show (1) the random variation decreases from micro-scale to macro-scale, and (2) the coefficient of variation in shear damage is larger than that in the tensile damage.

Keywords Statistical variations · Multi-scale · Damage evolution · Concrete · Micro-structure

S. Liang
School of Civil Engineering and Architecture, Zhejiang Sci-Tech University, Hangzhou 310018, People's Republic of China

J.-S. Chen (✉)
Department of Structural Engineering, University of California, San Diego, CA 92093, USA
e-mail: js-chen@ucsd.edu

J. Li
School of Civil Engineering, Tongji University, Shanghai 200092, People's Republic of China

S.-P. Lin
Research and Innovation Center, Ford Motor Company, Dearborn, MI 48124, USA

S.-W. Chi
Department of Civil and Materials Engineering, University of Illinois at Chicago, Chicago, IL 60607, USA

M. Hillman
Department of Civil and Environmental Engineering, The Pennsylvania State University, University Park, PA 16802, USA

M. Roth · W. Heard
U.S. Army Engineer Research and Development Center, Vicksburg, MS 39180, USA

1 Introduction

Concrete, as one of the key construction materials in engineering applications, is a complex composite material, and its properties have been investigated over a wide range of length scales from nanometers to meters. While typically treated as a homogeneous material at the continuum scale, the randomness in concrete constituents (aggregates, cement, etc.) and defects (micro-

cracks and micro-voids) have profound influence on its mechanical behavior. Understanding the variation of uncertainty in material parameters between scales in concrete has become an important and yet challenging problem.

As the general framework to link material properties between the micro-scale and macro-scale, Hill (1984) provided the basis for homogenization and multi-scale analysis. The work by Huet (1990, 1991) based on the partition theorem provided the hierarchies and bounds for size effects in the homogenized properties. For consideration of energy dissipation in solid mechanics, Ostoja-Starzewski (2001) provided the basis of the RVE under the framework of continuum thermodynamics. For representing microstructural randomness, the work in Ostoja-Starzewski (2001) introduced the concept of Statistical Volume Element (SVE). With the analogy of thermodynamics to continuum damage mechanics, the scaling of damage parameter was derived, and it was concluded that "The larger the specimen the more likely it is to fail", which is consistent with the Weibull-type representation of brittle solid (Bazant and Planas 1998).

In the area of multi-scale damage modeling, Fish et al. (1999) introduced a non-local damage theory based on asymptotic homogenization. Döbert et al. (2000) presented an anisotropic continuum damage material model to describe the macroscopic nonlinear behavior of fiber-reinforced composites. Dascalu et al. (2008) proposed a damage model to describe the size effect using an explicit description of elementary volumes with micro-cracks. Ren et al. (2011) proposed a micro-crack informed damage model, where Helmholtz free energy bridging is derived and utilized as the vehicle to relate the cracked micro-structure to the damaged macroscopic continuum.

The stochastic nature of concrete properties due to the high randomness in the micro-structures and the micro-voids has motivated research in the multi-scale methods that considers randomness on meso- and micro-scales. The asymptotic expansion has been modified with the first order stochastic perturbation method (Kamiński and Kleiber 2000) as well as with high order methods (Kamiński 2007; Sakata et al. 2008). Xu and Graham-Brady (2006) employed the Fourier Galerkin homogenization method to solve elliptic problems with random media. Xu (2007) introduced a polynomial chaos expansion based stochastic Galerkin method to establish a multi-scale model. Tootkaboni and Graham (2010) linked the macro-scale properties of multi-phase periodic composites to the random material properties of their microstructural components by the spectral stochastic computational scheme. Under the framework of multi-scale energy bridging method, Li and Ren (2011) obtained the stochastic damage evolution from the numerical simulation of micro-cells with random material properties. While these works provided the qualitative relation between random microstructure and homogeneous macro properties, little has been done on investigating and quantifying the relationship of randomness in material properties between scales.

In the present paper, we introduce a computational approach to quantify the relationship between the probability variation of micro-scale void size in concrete and the variation in macro-scale damage parameters using the homogenization based multi-scale damage model. The outline of the paper is as follows. In Sect. 2, a stochastic description, the probability distribution of micro-void radius, and the micro-void position (x coordinate and y coordinate) in a high strength concrete, is obtained by examining X-ray computed tomography (CT) scans of the concrete. In Sect. 3, the free energy bridging approach is introduced that links crack evolution at micro-scale to damage accumulation at macro-scale. Then, a generalized density evolution equation (GDEE) is applied to describe the nonlinear transportation of randomness between micro- and macro-scales in Sect. 4. Numerical examples are given in Sect. 5. In this section, the enriched Reproducing Kernel Particle Method (RKPM) is first reviewed, and the concrete micro-cells are generated with the consideration of the randomly distributed micro-voids from the CT scans. Micro-crack propagation in micro-cells with stochastic micro-structures is then simulated using RKPM, and the corresponding Helmholtz free energy histories are used to extract the stochastic tensile and shear damage evolutions using the energy bridging technique. Based on simulation results with stochastic micro-structures, coefficients of variation between micro- and macro-scales are estimated as the quantitative indices representing relation of randomness between the two scales. Concluding remarks of the presented investigation are given in Sect. 6.

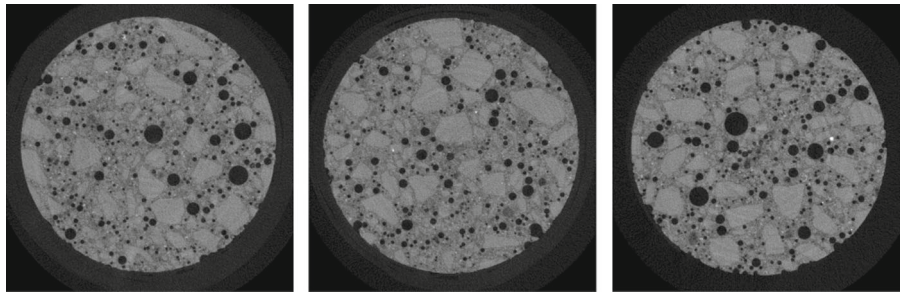

Fig. 1 CT scan samples of the high strength concrete

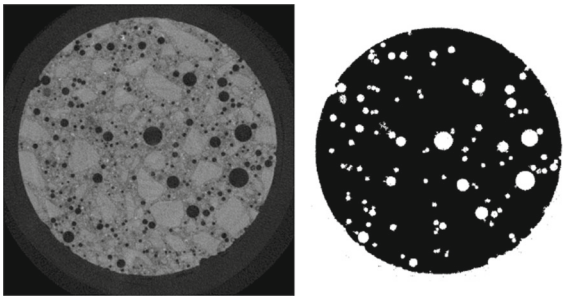

Fig. 2 Two-phase image of the concrete

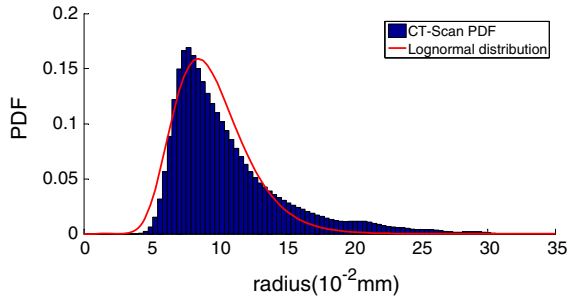

Fig. 3 PDF of the micro-void radius

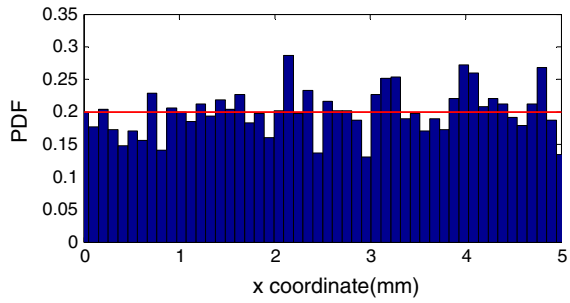

Fig. 4 PDF of the micro-void x-coordinate

2 Stochastic micro-structure of concrete

In this paper, CT scans are employed for characterization of the stochastic properties of high strength concrete (Heard 2014) at micro-scale. Figure 1 shows 3 CT scans among the 48 total considered. The diameter of all the concrete samples is 7.2 mm.

In high strength concrete, how the micro-voids nucleate and grow near the crack tip has stronger influence on the fracture process and failure mechanisms (Shah 1995). Therefore, we simplify the concrete into two phases, the matrix and the voids, where the reconstructed sample is given in Fig. 2. It can be observed in the samples that the radius and the position of the micro-voids both are randomly distributed and are considered here as the independent random variables.

Based on the distribution obtained from the CT scans, a lognormal distribution is chosen to represent the distribution of the micro-void radius R_v, where the probability of a micro-void with radius less than r is given as

$$f(r, \mu, \vartheta) = \frac{1}{r\vartheta\sqrt{2\pi}} e^{-(\ln r - \mu)^2/2\vartheta^2} \tag{1}$$

where μ is the logarithmic mean value and ϑ is the standard deviation of the radius, and for the scanned samples the values are $\mu = 2.2186 \times 10^{-2}$mm and $\vartheta = 0.2990$, respectively. Figure 3 shows the probability density function (PDF) of the radius along with the lognormal distribution. The PDF of the x-coordinate X_v and y-coordinate Y_v are plotted in Figs. 4, 5, respectively. Based on the statistical data of the x-coordinate and y-coordinate of the micro-voids in the samples, we assume a uniform distribution for the position of the micro-voids.

To describe the overall randomness on the micro-structure, the porosity is defined as

$$p_{mv} = \frac{A_{mv}}{A_{ct}} \tag{2}$$

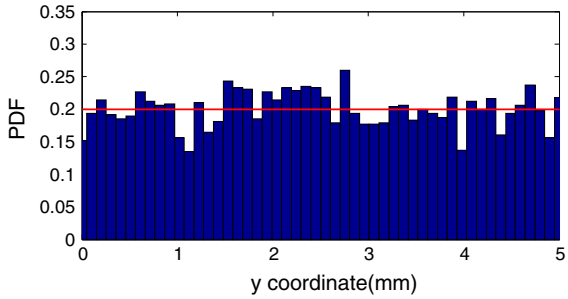

Fig. 5 PDF of the micro-void y-coordinate

where A_{mv} is the total area of the micro-voids; A_{ct} is the area of the sample under CT scan. The mean value and standard deviation of the porosity are obtained as $\mu_p = 0.0873$ and $\sigma_p = 0.0156$, respectively. Coefficient of variation (COV) of the porosity is introduced to quantify the variation of its randomness on the micro-structure as

$$C_{micro} = \frac{\sigma_p}{\mu_p} = 0.1787 \tag{3}$$

Based on the random variable description of the micro-voids, the two-phase geometry of the micro-cell can be generated for stochastic multi-scale analysis.

3 Homogenization based energy bridging between scales

The foundation of homogenization is that there exists an RVE if one of these two conditions is satisfied: (1) the micro-cell of the material is periodic, and (2) micro-cell volume contains a very large (mathematically infinite) set of microscopic elements where statistical homogeneity and ergodicity can be captured. In Ostoja-Starzewski (2001) and Ostoja-Starzewski (2006), the investigation was made based on the hierarchies of the meso-scale bounds together with the principle of minimum potential energy. Ostoja-Starzewski (2006) clarified that homogenization should meet the two bounds stemming from Dirichlet and Neumann boundary value problems for the random material, in which the stochastic representative volume element (SRVE) can be approximately transferred into the RVE. Lin et al. (2016) employed the energy bridging between cracked micro-structure and damaged continuum, and followed the pioneering work of Ostoja-Starzewski (2001) in deriving the scale effect of damage state. This work demonstrated how a stochastic damage model could be constructed using micro-crack information under the framework of SRVEs. With consideration of the stochastic micro-structure presented in Sect. 2, homogenization will be performed on the SRVE, and stochastic damage evolution functions will be extracted accordingly in the remaining part of this section.

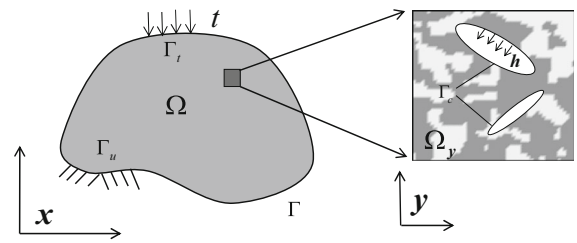

Fig. 6 Macro-structure and micro-cell

3.1 Homogenization method

Consider the macroscopic coordinate $\boldsymbol{x}$ and microscopic coordinate $\boldsymbol{y}$, where the transformation between $\boldsymbol{x}$ and $\boldsymbol{y}$ are defined by a small scale parameter λ:

$$\boldsymbol{y} = \frac{\boldsymbol{x}}{\lambda} \tag{4}$$

Within the domain Ω, the micro-cell Ω_y contains a distribution of arbitrary micro-cracks with the sum of all the crack surfaces Γ_c, as shown in Fig. 6.

Without loss of generality, the boundary value problem without body force is expressed as follows:

$$\nabla \cdot \boldsymbol{\sigma}^{\lambda} = 0 \text{ in } \Omega \tag{5}$$

$$\boldsymbol{\sigma}^{\lambda} \cdot \boldsymbol{n} = \boldsymbol{t} \text{ on } \Gamma_t \tag{6}$$

$$\boldsymbol{u}^{\lambda} = \bar{\boldsymbol{u}} \text{ on } \Gamma_u \tag{7}$$

$$\boldsymbol{\sigma}^{\lambda} \cdot \boldsymbol{n} = \boldsymbol{h} \text{ on } \Gamma_c \tag{8}$$

where $\boldsymbol{\sigma}^{\lambda}$ is the total stress, the superscript "λ" represents the total solution combining the coarse and fine scales, $\boldsymbol{n}$ is the surface normal vector, $\boldsymbol{u}^{\lambda}$ is the total displacement, $\bar{\boldsymbol{u}}$ is the prescribed displacement on the surface Γ_u, $\boldsymbol{t}$ is the surface traction on Γ_t and h is the surface traction on Γ_c. The total strain can be expressed as

$$\boldsymbol{\varepsilon}^{\lambda} = \frac{1}{2}\left(\nabla \otimes \boldsymbol{u}^{\lambda} + \boldsymbol{u}^{\lambda} \otimes \nabla\right) \tag{9}$$

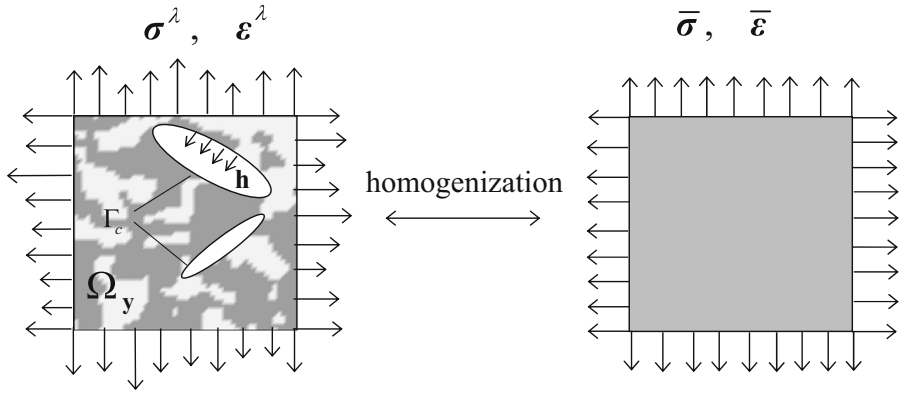

Fig. 7 Homogenization of micro-cell

To solve Eqs. (5)–(8) directly, all the details of the micro-structures and heterogeneities involving in the domain Ω should be considered, which is computationally infeasible. Alternatively, homogenized medium using a representative micro-cell as shown in Fig. 7, with tractions and displacements acting on the micro-cell boundaries is considered.

The homogenized stress and strain in the homogenized continuum are defined based on the tractions and displacements prescribed on the outer boundary of the micro-cell (Ren et al. 2011) as follows:

$$\bar{\boldsymbol{\sigma}} = \frac{1}{V_y}\oint_{\partial\Omega_y}\left(\boldsymbol{t}^{\lambda}\otimes\boldsymbol{x}\right)\mathrm{d}\Omega \tag{10}$$

$$\bar{\boldsymbol{\varepsilon}} = \frac{1}{2V_y}\oint_{\partial\Omega_y}\left(\boldsymbol{u}^{\lambda}\otimes\boldsymbol{n}+\boldsymbol{n}\otimes\boldsymbol{u}^{\lambda}\right)\mathrm{d}\Gamma \tag{11}$$

where V_y is the volume of the micro-cell; $\boldsymbol{t}^{\lambda}$ is the traction which combines the coarse and fine scale components (Ren et al. 2011). Introducing the averaging operator $\langle\cdot\rangle = \frac{1}{V_y}\int_{\Omega_y}\cdot\,\mathrm{d}\Omega$, the averaged stress and strain in the cracked micro-cell are defined as

$$\left\langle\boldsymbol{\sigma}^{\lambda}\right\rangle = \frac{1}{V_y}\int_{\Omega_y}\boldsymbol{\sigma}^{\lambda}\mathrm{d}\Omega \tag{12}$$

$$\left\langle\boldsymbol{\varepsilon}^{\lambda}\right\rangle = \frac{1}{V_y}\int_{\Omega_y}\boldsymbol{\varepsilon}^{\lambda}\mathrm{d}\Omega \tag{13}$$

Note that the following equality exists for the case without body force:

$$\nabla\cdot\left(\boldsymbol{\sigma}^{\lambda}\otimes\boldsymbol{x}\right) = \nabla\cdot\boldsymbol{\sigma}^{\lambda}\otimes\boldsymbol{x}+\boldsymbol{\sigma}^{\lambda}\cdot(\nabla\otimes\boldsymbol{x}) = \boldsymbol{\sigma}^{\lambda} \tag{14}$$

Substituting Eqs. (14) into (12), one can obtain the relationship between the averaged stress and homogenized stress in the micro-cell:

$$\begin{aligned}\left\langle\boldsymbol{\sigma}^{\lambda}\right\rangle &= \frac{1}{V_y}\int_{\Omega_y}\boldsymbol{\sigma}^{\lambda}\mathrm{d}\Omega\\ &= \frac{1}{V_y}\int_{\Omega_y}\nabla\cdot\left(\boldsymbol{\sigma}^{\lambda}\otimes\boldsymbol{x}\right)\mathrm{d}\Omega\\ &= \frac{1}{V_y}\oint_{\partial\Omega_y}\left(\boldsymbol{t}^{\lambda}\otimes\boldsymbol{x}\right)\mathrm{d}\Gamma-\frac{1}{V_y}\oint_{\Gamma_c}\left(\boldsymbol{t}^{\lambda}\otimes\boldsymbol{x}\right)\mathrm{d}\Gamma\\ &= \bar{\boldsymbol{\sigma}}-\frac{1}{V_y}\oint_{\Gamma_c}\left(\boldsymbol{t}^{\lambda}\otimes\boldsymbol{x}\right)\mathrm{d}\Gamma\end{aligned} \tag{15}$$

Considering equilibrium of the cohesive stress on the crack surface, the second term of the right side of Eq. (15) drops and Eq. (15) can be further simplified as

$$\bar{\boldsymbol{\sigma}} = \left\langle\boldsymbol{\sigma}^{\lambda}\right\rangle \tag{16}$$

Substituting Eqs. (14) into (13), the relationship between the averaged strain and homogenized strain is as follows:

$$\begin{aligned}\left\langle\boldsymbol{\varepsilon}^{\lambda}\right\rangle &= \frac{1}{V_y}\int_{\Omega_y}\boldsymbol{\varepsilon}^{\lambda}\mathrm{d}\Omega\\ &= \frac{1}{2V_y}\int_{\Omega_y}\left(\nabla\otimes\boldsymbol{u}^{\lambda}+\boldsymbol{u}^{\lambda}\otimes\nabla\right)\mathrm{d}\Omega\\ &= \frac{1}{2V_y}\oint_{\partial\Omega_y}\left(\boldsymbol{n}\otimes\boldsymbol{u}^{\lambda}+\boldsymbol{u}^{\lambda}\otimes\boldsymbol{n}\right)\mathrm{d}\Gamma\\ &\quad-\frac{1}{2V_y}\oint_{\Gamma_c}\left(\boldsymbol{n}\otimes\boldsymbol{u}^{\lambda}+\boldsymbol{u}^{\lambda}\otimes\boldsymbol{n}\right)\mathrm{d}\Gamma\\ &= \bar{\boldsymbol{\varepsilon}}-\frac{1}{2V_y}\oint_{\Gamma_c}\left(\boldsymbol{n}\otimes\boldsymbol{u}^{\lambda}+\boldsymbol{u}^{\lambda}\otimes\boldsymbol{n}\right)\mathrm{d}\Gamma\end{aligned} \tag{17}$$

or

$$\bar{\boldsymbol{\varepsilon}} = \left\langle\boldsymbol{\varepsilon}^{\lambda}\right\rangle+\frac{1}{2V_y}\oint_{\Gamma_c}\left(\boldsymbol{n}\otimes\boldsymbol{u}^{\lambda}+\boldsymbol{u}^{\lambda}\otimes\boldsymbol{n}\right)\mathrm{d}\Gamma \tag{18}$$

With the presence of displacement discontinuity across the micro-cracks, the homogenized strain differs from the averaged strain in the micro-cell.

3.2 Energy bridging between cracked micro-structure and damage continuum

Ren et al. (2011) introduced an energy bridging method to obtain the damage evolution functions from cracked micro-structures as discussed in the next sub-section. The Helmholtz free energy (HFE) is used to relate the strain energy in the cracked micro-structure and the damaged homogenized continuum. The Helmholtz free energy (HFE) in the micro-structure is defined as

$$\psi^{\lambda} = \frac{1}{2}\boldsymbol{\sigma}^{\lambda} : \boldsymbol{\varepsilon}^{\lambda} \tag{19}$$

In the homogenized continuum, the HFE can be expressed as

$$\bar{\psi} = \frac{1}{2}\bar{\boldsymbol{\sigma}} : \bar{\boldsymbol{\varepsilon}} \tag{20}$$

Ren et al. (2011) derived the relationship between the HFE of the homogenized material to the HFE in the cracked micro-structure as

$$\bar{\psi} = \frac{1}{V_y}\left(\int_{\Omega_y} \psi^{\lambda} \mathrm{d}\Omega + \frac{1}{2}\oint_{\Gamma_c} \boldsymbol{u}^{\lambda} \cdot \boldsymbol{h} \mathrm{d}\Gamma\right) \tag{21}$$

This HFE relationship between a cracked micro-structure and homogenized damaged continuum can be used to extract the damage evolution functions of various damage models (Ren et al. 2011). In this study, the volumetric-deviatoric decomposition (Bazant et al. 2000; Adley et al. 2010) is adopted to describe the different damage mechanism of concrete. It is assumed that in the volumetric space the concrete damage is activated by the tensile damage mechanism, while in the deviatoric space the concrete damage is activated by the shear damage mechanism (Lin et al. 2016).

To demonstrate, consider the undamaged elastic constitutive law

$$\bar{\boldsymbol{\sigma}}_0 = \bar{C}_0 : \bar{\boldsymbol{\varepsilon}} \tag{22}$$

where the subscript "0" represents the undamaged state.

A decomposition of the effective stress tensor can be expressed as

$$\bar{\boldsymbol{\sigma}}_0 = \bar{\boldsymbol{\sigma}}_0^{vol} + \bar{\boldsymbol{\sigma}}_0^{dev} \tag{23}$$

where the term "*dev*" represents deviatoric and "*vol*" represents volumetric.

Based on the volumetric-deviatoric decomposition, the Helmholtz free energy then can be expressed as

$$\bar{\psi} = (1 - d^t)\psi_0^{vol} + (1 - d^s)\psi_0^{dev} \tag{24}$$

where d^t and d^s are the tensile and shear scalar damage parameters, respectively, ψ_0^{vol},ψ_0^{dev} are the volumetric and deviatoric effective Helmholtz free energies, respectively, defined as

$$\psi_0^{vol} = \frac{1}{2}\bar{\boldsymbol{\sigma}}^{vol} : \overline{\boldsymbol{C}}_0^{-1} : \bar{\boldsymbol{\sigma}}^{vol} \tag{25}$$

$$\psi_0^{dev} = \frac{1}{2}\bar{\boldsymbol{\sigma}}^{dev} : \overline{\boldsymbol{C}}_0^{-1} : \bar{\boldsymbol{\sigma}}^{dev} \tag{26}$$

By computing the HFE $\bar{\psi}$ in the cracked micro-structure using Eq. (21) (see Ren et al. 2011 for details), the damage evolution function can then be obtained as follows

$$d^t = 1 - \frac{\partial\bar{\psi}}{\partial\psi_0^{vol}} \approx 1 - \frac{\Delta\bar{\psi}}{\Delta\psi_0^{vol}} \tag{27}$$

$$d^s = 1 - \frac{\partial\bar{\psi}}{\partial\psi_0^{dev}} \approx 1 - \frac{\Delta\bar{\psi}}{\Delta\psi_0^{dev}} \tag{28}$$

Applications to extracting damage evolution functions for other damage models can also be done (see Ren et al. 2011; Li and Ren 2011). In the present study, Eqs. (27) and (28) are employed to obtain the damage evolution functions for concrete materials.

4 Generalized density evolution equation

To effectively obtain a probability description of the homogenized stress–strain relationship as well as the variation in damage evolution due to the statistical variations of microstructures, we consider the generalized density evolution equations (GDEE) for PDF of state variables in arbitrary dimension (Li and Chen 2007, 2008; Chen and Li 2009). The principle of preservation of probability (Gibbs 2010) states that in a fixed domain of the state space, the increment of probability during a time interval is equal to the probability transited through the bounds during the same time interval. The generalized density evolution equation can be derived from the principle of preservation of probability.

Without loss of generality, a monotonic stress–strain relationship with initial conditions is considered:

$$\sigma = g(\Theta, d, \varepsilon)\,,\ \sigma(\varepsilon_0) = \sigma_0 \tag{29}$$

where ε_0 is the initial value of strain, σ_0 is the initial value of stress and Θ is the random parameter vector whose joint probability density function is $p_\Theta(\boldsymbol{\theta})$ with $\boldsymbol{\theta}$ the realization associated with Θ. In the micro-cells from the CT scans, we define $\Theta = (R_v, X_v, Y_v)$ representing the randomness in the dimension and the x- and y- positions of voids.

Similarly, damage state can also be considered as a function of the input random variables and the strain as

$$d = f(\Theta, \varepsilon)\,,\ d(\varepsilon_0) = d_0 \tag{30}$$

where d_0 is the initial value of the damage. In this study, the initial condition is an undamaged state $d_0 = 0$. The damage rate with respect to strain is expressed as

$$\frac{\partial d}{\partial \varepsilon} = \frac{\partial f(\Theta, \varepsilon)}{\partial \varepsilon} = h(\Theta, \varepsilon) \tag{31}$$

The conditional transition PDF of d under the condition $\{\Theta = \boldsymbol{\theta}\}$ is defined as $p_{d|\Theta}\left(\widehat{d},\, \varepsilon \,|\, \boldsymbol{\theta}\right)$, where $d = \widehat{d}$ is a realization in the probability space, and $0 \le \widehat{d} \le 1$ is the range of the possible values of damage d. Under the condition $\{\Theta = \boldsymbol{\theta}\}$, there exists $\widehat{d}(\varepsilon) = f(\boldsymbol{\theta}, \varepsilon)$. It is equivalent to say that the following equations are satisfied for the conditional transition PDF as

$$p_{d|\Theta}\left(\widehat{d},\, \varepsilon \,|\, \boldsymbol{\theta}\right) = 0,\ \widehat{d} \neq f(\boldsymbol{\theta}, \varepsilon) \tag{32}$$

$$p_{d|\Theta}\left(\widehat{d},\, \varepsilon \,|\, \boldsymbol{\theta}\right) = \infty,\ \widehat{d} = f(\boldsymbol{\theta}, \varepsilon) \tag{33}$$

Additionally,

$$\int_{-\infty}^{+\infty} p_{d|\Theta}\left(\widehat{d},\, \varepsilon \,|\, \boldsymbol{\theta}\right) d\boldsymbol{\theta} = 1 \tag{34}$$

Combining Eqs. (32)–(34), the conditional transition PDF of the damage can be expressed as

$$p_{d|\Theta}\left(\widehat{d},\, \varepsilon \,|\, \boldsymbol{\theta}\right) = \delta\left(\widehat{d} - f(\boldsymbol{\theta}, \varepsilon)\right) \tag{35}$$

where $\delta(\cdot)$ is the Dirac delta function.

Taking the derivative of Eq. (35) on both sides, it yields

$$\begin{aligned}
\frac{\partial p_{d|\Theta}\left(\widehat{d},\, \varepsilon \,|\, \boldsymbol{\theta}\right)}{\partial \varepsilon} &= \frac{\partial \delta\left(\widehat{d} - f(\boldsymbol{\theta}, \varepsilon)\right)}{\partial \varepsilon} \\
&= \left[\frac{\partial \delta(y)}{\partial y}\right]_{y=\widehat{d}-f(\boldsymbol{\theta},\varepsilon)} \cdot \frac{\partial\left(\widehat{d} - f(\boldsymbol{\theta}, \varepsilon)\right)}{\partial \varepsilon} \\
&= \frac{\partial\left\{\delta\left[\widehat{d} - f(\boldsymbol{\theta}, \varepsilon)\right]\right\}}{\partial\, \widehat{d}} \cdot \frac{\partial\, \widehat{d}}{\partial y} \cdot \frac{\partial\left(\widehat{d} - f(\boldsymbol{\theta}, \varepsilon)\right)}{\partial \varepsilon} \\
&= \frac{\partial\left\{\delta\left[\widehat{d} - f(\boldsymbol{\theta}, \varepsilon)\right]\right\}}{\partial\, \widehat{d}} \cdot \frac{\partial\left(\widehat{d} - f(\boldsymbol{\theta}, \varepsilon)\right)}{\partial \varepsilon} \\
&= \frac{\partial\left\{\delta\left[\widehat{d} - f(\boldsymbol{\theta}, \varepsilon)\right]\right\}}{\partial\, \widehat{d}} \cdot \left[-\frac{\partial f(\boldsymbol{\theta}, \varepsilon)}{\partial \varepsilon}\right] \\
&= -h(\boldsymbol{\theta}, \varepsilon) \cdot \frac{\partial p_{d|\Theta}\left(\widehat{d},\, \varepsilon \,|\, \boldsymbol{\theta}\right)}{\partial\, \widehat{d}}
\end{aligned} \tag{36}$$

According to the conditional PDF formula, the joint PDF of $p_{d\Theta}\left(\widehat{d}, \varepsilon, \boldsymbol{\theta}\right)$ reads:

$$p_{d\Theta}\left(\widehat{d}, \varepsilon, \boldsymbol{\theta}\right) = p_{d|\Theta}\left(\widehat{d},\, \varepsilon \,|\, \boldsymbol{\theta}\right) p_\Theta(\boldsymbol{\theta}) \tag{37}$$

Multiplying $p_\Theta(\boldsymbol{\theta})$ on both sides of Eq. (36), the GDEE for the damage evolution can be formed as

$$\frac{\partial p_{d\Theta}\left(\widehat{d}, \varepsilon, \boldsymbol{\theta}\right)}{\partial \varepsilon} + h(\boldsymbol{\theta}, \varepsilon) \cdot \frac{\partial p_{d\Theta}\left(\widehat{d}, \varepsilon, \boldsymbol{\theta}\right)}{\partial\, \widehat{d}} = 0 \tag{38}$$

From Eqs. (36)–(38), the initial condition can be rewritten as

$$p_{d\Theta}\left(\widehat{d}, \varepsilon_0, \boldsymbol{\theta}\right) = \delta(\widehat{d} - \widehat{d_0}) p_\Theta(\boldsymbol{\theta}) \tag{39}$$

After obtaining the damage rate $h(\boldsymbol{\theta}, \varepsilon)$ for each sample based on the modeling of cracked micro-cell and the energy bridging approach to obtain the damage evolution function $d(\varepsilon)$ as discussed in Sect. 3, we can solve the joint probability density function of the damage $p_{d\Theta}\left(\widehat{d}, \varepsilon, \boldsymbol{\theta}\right)$ in Eq. (38) numerically. The PDF of $d(\varepsilon)$, $p_d\left(\widehat{d}, \varepsilon\right)$ can then be obtained by

$$p_d\left(\widehat{d}, \varepsilon\right) = \int_{\Omega_\Theta} p_{d\Theta}\left(\widehat{d}, \varepsilon, \boldsymbol{\theta}\right) \mathrm{d}\boldsymbol{\theta} \tag{40}$$

The procedure to obtain the PDF of $d(\varepsilon)$ is summarized as follows:

(1) Select a discretized representative point set $\theta_q = \left(\theta_{1q}, \boldsymbol{\theta}_{2q}, \ldots, \theta_{nq}\right), q = 1, 2, \ldots, M$ in the domain $\Omega = \Omega_\theta$; where n is the dimension of the random vector and M is the total number of the selected points. Note that the representative points can be obtained by the quasi-symmetric point method or by hyperball sieving techniques (Xu et al. 2012).

(2) For the prescribed $\boldsymbol{\theta}_q$, generate the corresponding micro-cell by the input random variables given in Sect. 2

(3) Propagation in each micro-cell subjected to tension and shear using enriched RKPM (Moës et al. 1999; Moës and Belytschko 2002). Then, obtain the homogenized HFE by the multi-scale energy bridging in Eq. (21) and obtain the damage evolution functions from Eq. (24). Calculate the derivative $\partial d/\partial\varepsilon$ by the finite difference method.

(4) Introduce $h(\Theta, \varepsilon) = \partial d/\partial\varepsilon$ into the generalized density evolution equation Eq. (36), and solve Eq. (38) under the initial condition Eq. (39) with the total variation diminishing (TVD) finite difference scheme (Li and Chen 2004) to obtain the numerical solution of $p_{d\Theta}(d, \varepsilon_0, \theta)$.

(5) Repeat step (3) and (4) for $q = 1, 2, \ldots, M$ and take numerical integration regarding θ_q to obtain PDF, i.e., $p_d(d, \varepsilon) = \int_{\Omega_\Theta} p_{d\Theta}(d, \boldsymbol{\theta}, \varepsilon)\, \mathrm{d}\boldsymbol{\theta} = \sum_{q=1}^{M} p_{d\Theta_q}\left(d, \boldsymbol{\theta}_q, \varepsilon\right)$.

5 Numerical examples

5.1 Fracture modeling using enriched RKPM

Conventional monomial-based approximation methods cannot effectively represent the nature of singularities and discontinuities of cracks. In this paper, the extrinsically enriched reproducing kernel particle method (RKPM) is adopted for the micro-cell analysis to model the singularities and discontinuities in the cracking process. The general expression of extrinsic enrichment methods (Moës et al. 1999; Moës and Belytschko 2002) for each component of displacement fields is

$$\boldsymbol{u}^h(\boldsymbol{x}) = \sum_{I\in N} \Psi_I(\boldsymbol{x})\, \boldsymbol{c}_I + \sum_{J\in N_{cut}} H(\boldsymbol{x})\, \Psi_J(\boldsymbol{x})\, \boldsymbol{a}_J + \sum_{K\in N_{tip}} \Psi_K(\boldsymbol{x}) \left(\sum_{i}^{3} \boldsymbol{b}_{iK} f_i(\boldsymbol{x})\right) \tag{41}$$

Here, $\boldsymbol{u}^h(\boldsymbol{x})$ is the displacement vector; $\mathbf{c}_I$, $\mathbf{a}_J$ and $\mathbf{b}_{iK}$ are the generalized coefficient vectors to be determined, $\Psi_I(\boldsymbol{x})$ is the conventional reproducing kernel (RK) shape function (Liu et al. 1995; Chen et al. 1996) possessing reproducibility of polynomials, N is the total number of nodes, N_{cut} is the number of the enriched nodes whose supports are cut through by the crack surface, and N_{tip} is the number of the near-tip enriched nodes whose supports cover the crack tip, and $H(\boldsymbol{x})$ is the sign function defined as:

$$H(\boldsymbol{x}) = \begin{cases} 1 & \hat{y} > 0 \\ 0 & \hat{y} = 0 \\ -1 & \hat{y} < 0 \end{cases} \tag{42}$$

where $\hat{y}$ is the local coordinate aligned with the crack surface as plotted in Fig. 8.

In this work, the cohesive zone model (Moës and Belytschko 2002) is chosen to describe fracture of the RVE. The enrichment function is put forward as follows

$$\{f_i(\boldsymbol{x})\} = \boldsymbol{f}(r, \theta) = \left\{ r\sin\left(\frac{\theta}{2}\right), r^{\frac{3}{2}}\sin\left(\frac{\theta}{2}\right), r^2\sin\left(\frac{\theta}{2}\right)\right\} \tag{43}$$

Note that the displacement bases with gradient singularities at the crack tip are not considered here due to the employment of cohesive zone model.

In order to impose essential boundary conditions for the meshfree method which does not have Kronecker delta properties, the following functional of the micro-cell problem is introduced

$$\Pi = \frac{1}{2}\int_{\Omega_y} \varepsilon_{ij} C_{ijkl} \varepsilon_{kl} d\Omega - \int_{\Gamma_t} u_i \bar{t}_i d\Gamma + \frac{\alpha}{2}\int_{\Gamma_u} (u_i - \bar{u}_i)(u_i - \bar{u}_i)\, d\Gamma \tag{44}$$

where Ω_y is the domain of the micro-cell, Γ_t and Γ_u are the associated natural boundary (including the crack surfaces) and the essential boundary, respectively, and α is the penalty parameter for imposing the essential boundary conditions. In the simulation, α is chosen as $(10^3 \sim 10^6)E$, where E is the Young's modulus. Taking the stationary condition of the functional in Eq. (44) and introducing the enriched RK approximation in

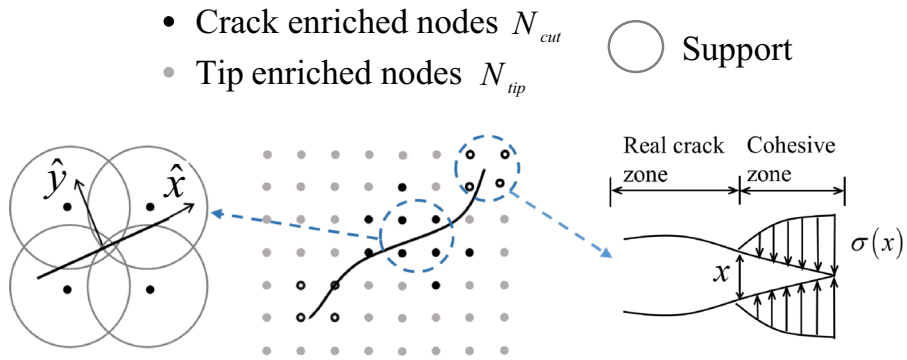

Fig. 8 Formulation of extrinsically enriched RKPM

Eq. (41) for the approximation of displacement field, the matrix form of the equation can be obtained as

$$(\boldsymbol{K} + \alpha \boldsymbol{K}_u)\, \boldsymbol{U} = \boldsymbol{F} + \alpha \boldsymbol{F}_u \tag{45}$$

where $\boldsymbol{K}$ is the stiffness matrix, $\boldsymbol{F}$ is the force vector; $\boldsymbol{K}_u$ and $\boldsymbol{F}_u$ are the terms associated with the imposition of essential boundary conditions.

5.2 Micro-cell generation

Based on Sect. 2, micro-cells with micro-voids having random radius and position are generated. The dimension of the micro-cell is adopted as 5 mm × 5 mm, which is the size cut from the actual circular shaped samples with diameter of 7.2 mm as shown in Sect. 2. The quasi-symmetric point method (Xu et al. 2012) is used to generate the random micro-void radius, and the micro-void x coordinate and y coordinate. The number of samples is taken to be 100. Figure 9 shows one sample of the micro-cell.

To obtain the uniaxial tensile and shear damage evolution functions in Eq. (27), the pure Dirichlet uni-axial tensile boundary condition and the pure shear boundary condition are imposed on the model as shown in Fig. 10.

5.3 Simulation results

According to laboratory test data (Heard 2014) the Young's modulus and Poisson's ratio of the micro-cell matrix are taken to be $E = 24.5$ GPa, $\upsilon = 0.16$, respectively, and the effective tensile strength is taken to be $f_t = 4.5\,\text{N/mm}^2$. The fracture energy for tension of the micro-cell is chosen as $G_f = 124\,\text{J/m}^2$ and the shear

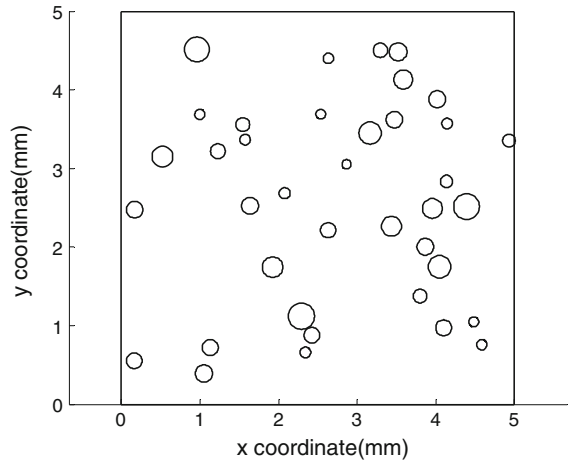

Fig. 9 Reconstructed micro-cell sample based on micro-voids statistical properties

fracture energy is chosen as $G_s = 2G_f$ (Lin et al. 2016). After the construction of the micro-cell model, the enriched RKPM as given in Sect. 5 is applied to simulate the crack propagation in each micro-cell sample and to obtain the stress, strain, and HFE histories. The boundary conditions prescribed on the cell boundary are illustrated in Fig. 10. The crack propagation in a micro-cell at different loading stages in the tensile and shear tests are shown in Figs. 11 and 12, respectively, where $\boldsymbol{u}_m$ denotes maximum prescribed displacement.

Using the simulation results, the homogenized stress–strain relationship, the associated HFEs, and the tensile and shear damage evolution functions of each micro-cell are obtained based on Eqs. (21), (27) and (28). The tensile homogenized stress–strain curves and damage evolution functions are depicted in Fig. 13a, b, respectively, and those for shear deformation are shown in Fig. 14a, b.

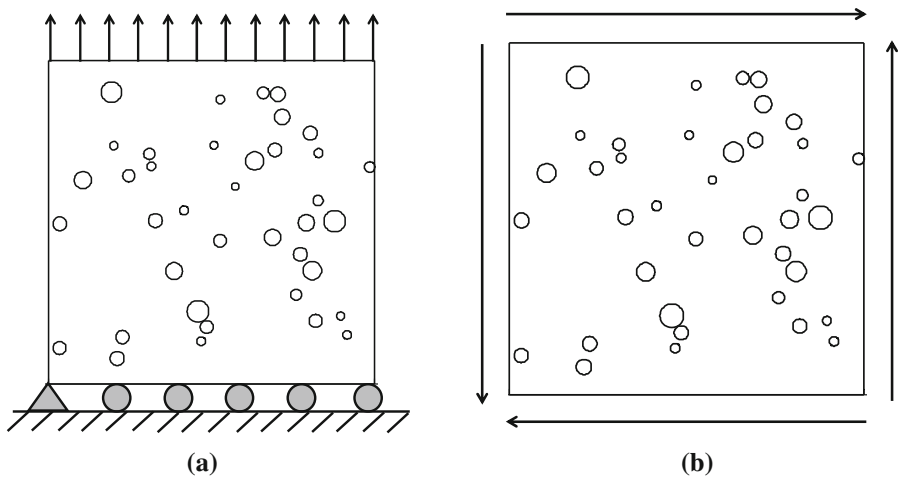

Fig. 10 Applied boundary conditions on the micro-cells. **a** uniaxial tension, **b** pure shear

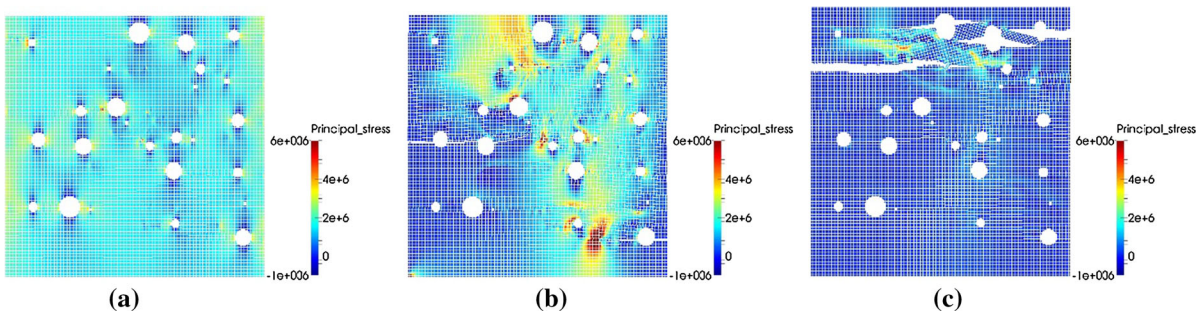

Fig. 11 Crack propagation of micro-cell under tensile test (Sample 76). **a** $\boldsymbol{u} = 0.3\boldsymbol{u}_m$, **b** $\boldsymbol{u} = 0.6\boldsymbol{u}_m$, **c** $\boldsymbol{u} = \boldsymbol{u}_m$

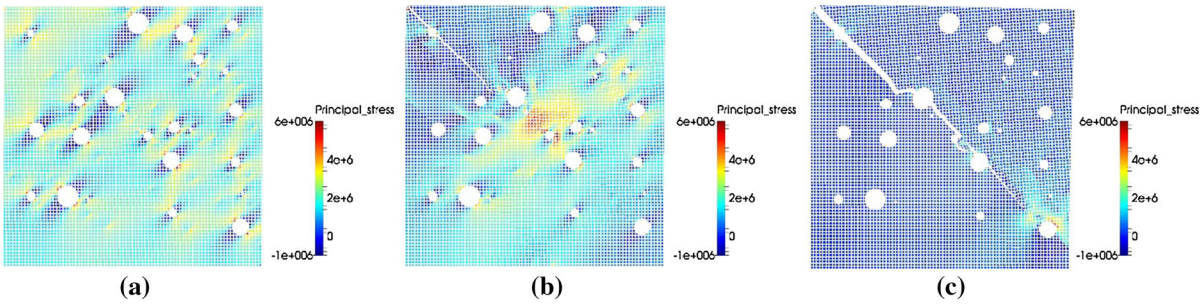

Fig. 12 Crack propagation of micro-cell under shear test (Sample 76). **a** $\boldsymbol{u} = 0.3\boldsymbol{u}_m$, **b** $\boldsymbol{u} = 0.6\boldsymbol{u}_m$, **c** $\boldsymbol{u} = \boldsymbol{u}_m$

For each micro-cell, the damage rate $h(\boldsymbol{\theta}, \varepsilon)$ is computed by the finite difference method, and by substituting it into the GDEE in Eqs. (38)–(40) the evolution of the probability density function of tensile and shear damage functions can then be obtained as shown in Figs. 15 and 16, respectively. The tensile and shear damage PDFs at selected strains are shown in Figs. 17 and 18, respectively.

Figures 17, 18 show how the PDFs of both the tensile and shear damage variables vary with the strains. It is evident that the distribution of the PDF is complex over a strain interval, especially after the cracks propagate. At some strain levels, the PDFs have two or more peaks, which implies the presence of random bifurcations during the response process. The computed mean value μ_d and the standard deviation (STD) σ_d of the

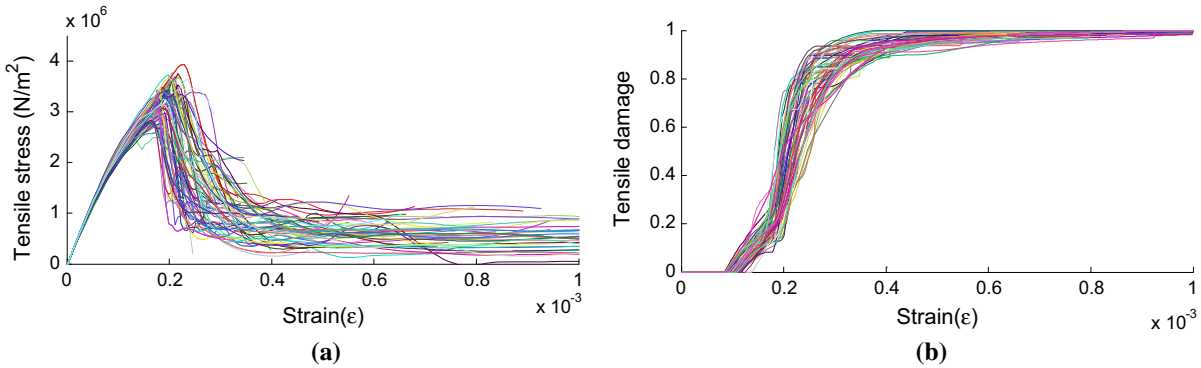

Fig. 13 Micro-cell analysis under uniaxial tensile boundary conditions. **a** Homogenized stress–strain relationship, **b** tensile damage

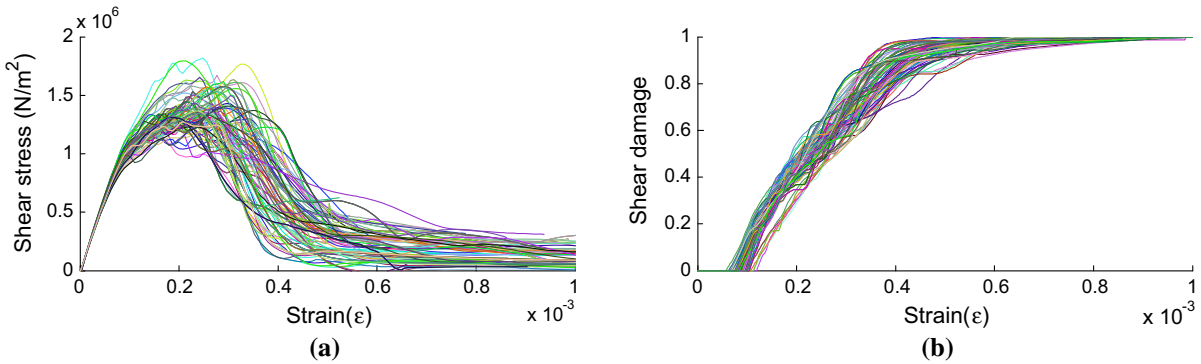

Fig. 14 Micro-cell analysis under pure shear boundary conditions. **a** Homogenized stress–strain relationship, **b** shear damage

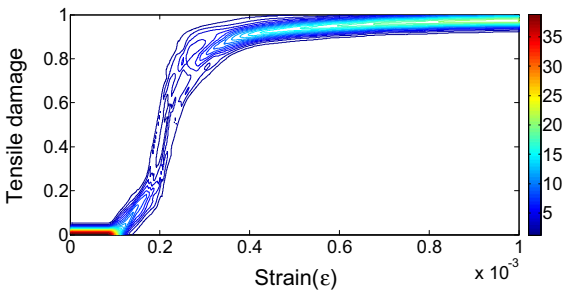

Fig. 15 Probability density contour of the tensile damage

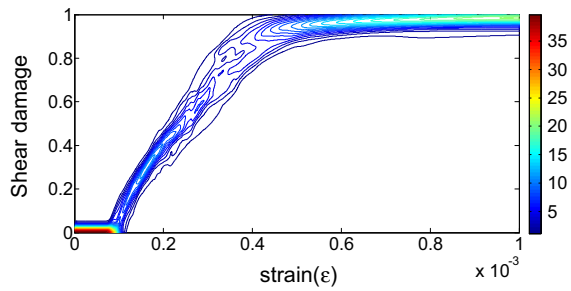

Fig. 16 Probability density contour of the shear damage

tensile and shear damages are also shown in Figs. 19, 20.

To further investigate the effects of microstructural randomness on the stochastic macroscopic properties, the coefficients of variation are introduced for tensile and shear damages. It should be noted that the damage evolution is a random process, so that the COV is not one single value corresponding to a given strain. Thus, we define the mean COV over the entire strain range to describe the variation (or the fluctuation) of randomness on the macro-scale as follows

$$C^t_{macro} = \frac{\bar{\sigma}^t_d}{\bar{\mu}^t_d}, \quad C^s_{macro} = \frac{\bar{\sigma}^s_d}{\bar{\mu}^s_d} \tag{46}$$

where $\bar{\sigma}^t_d$ and $\bar{\sigma}^s_d$ denotes the averaged STD of the random damage process in tension and shear, respec-

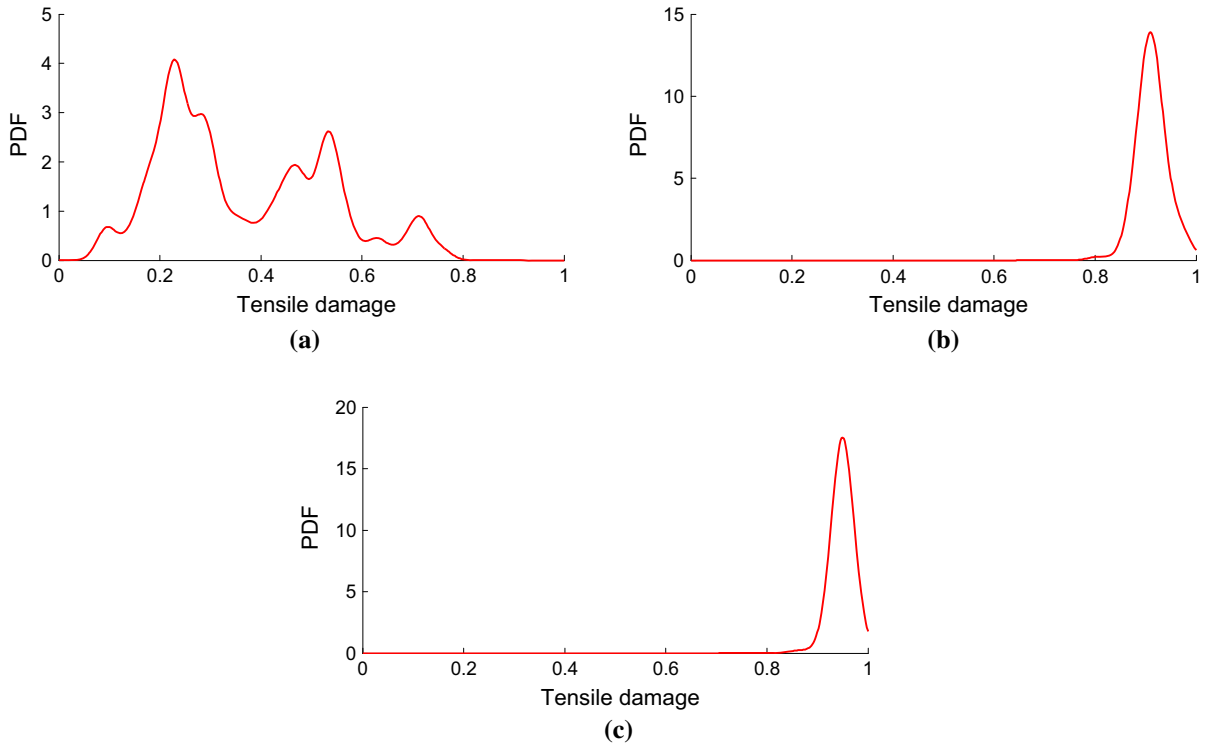

Fig. 17 PDF of the tensile damage on certain strain. **a** $\varepsilon = 0.0002$, **b** $\varepsilon = 0.0004$, **c** $\varepsilon = 0.0006$

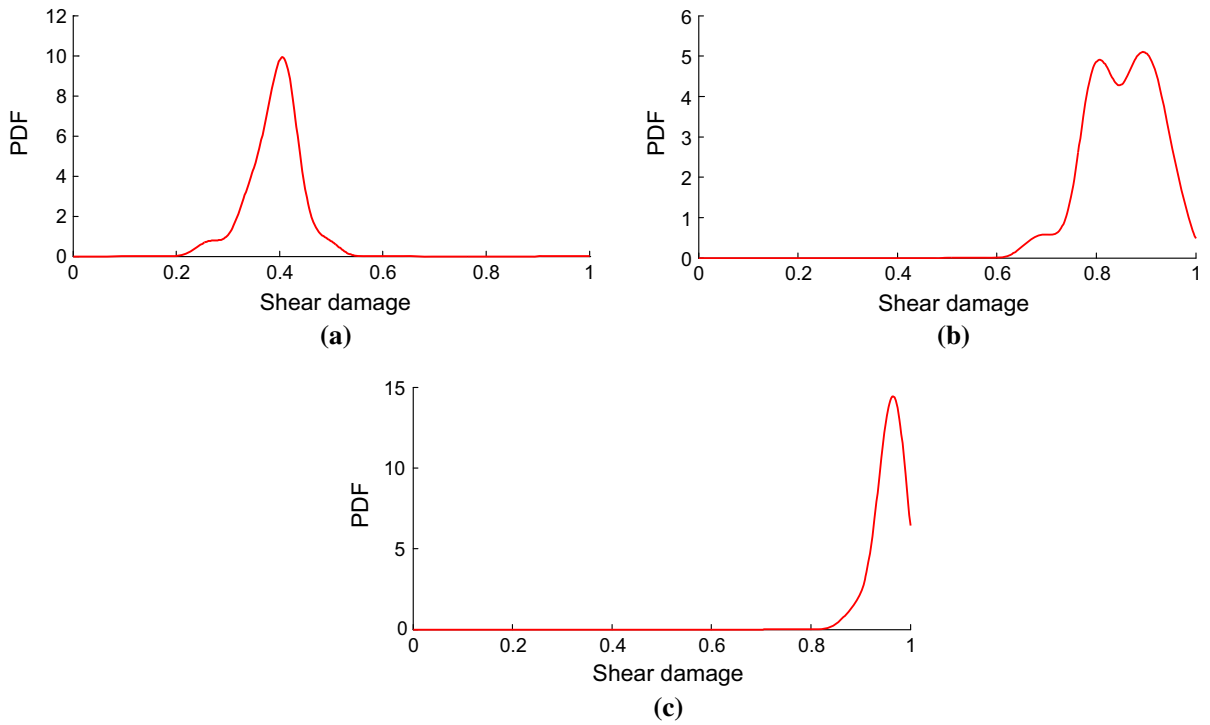

Fig. 18 PDF of the shear damage on certain strain. **a** $\varepsilon = 0.0002$, **b** $\varepsilon = 0.0004$, **c** $\varepsilon = 0.0006$

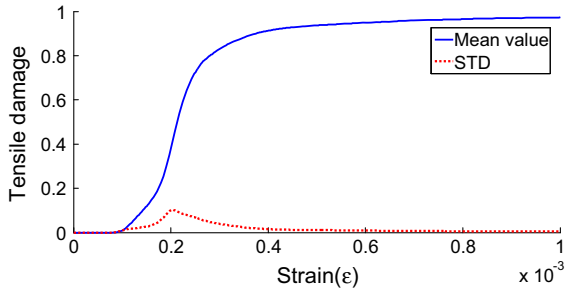

Fig. 19 Mean and STD for tensile damage

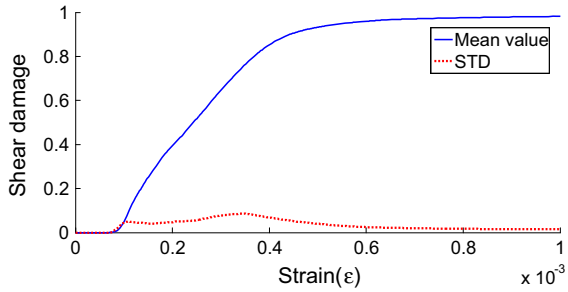

Fig. 20 Mean and STD for shear damage

tively, and $\bar{\mu}_d^t$ and $\bar{\mu}_d^s$ denote the corresponding averaged mean values of damages, respectively.

For the tensile damage $C_{macro}^t = 0.0239$, and for shear damage $C_{macro}^s = 0.0477$. Taking the COV on the micro-scale defined in Eq. (3) into consideration, we define the relative COV between different scales as

$$C_r^t = \frac{C_{macro}^t}{C_{micro}^t}, \quad C_r^s = \frac{C_{macro}^s}{C_{micro}^s} \tag{47}$$

Equation (47) can be understood as a ratio of the randomness between macro and micro scales. In this study, the relative COVs for the tensile and shear damages are:

$$C_r^t = \frac{0.0239}{0.1787} = 0.1337, C_r^s = \frac{0.0477}{0.1787} = 0.2669 \tag{48}$$

It is obvious that in Eq. (48) the random variation decreases from micro-scale to macro-scale. Also, it is interesting to observe in the simulation results that the COV in shear damage is larger than that in the tensile damage even for the same micro-cell geometries and identical material parameters. This shows how the different fracture processes and modes due to different loading conditions play an important role in the randomness transmission to large scales, which deserves further study.

5.4 Model validation

For validation purposes, the numerical simulation of tri-axial compression on cylindrical concrete specimens is performed. The concrete cylinder in the experiment (Heard 2014) is 100 mm in diameter and 200 mm in height. Confinement is applied to the outer surface of the cylinder with pressure of 100 MPa, and vertical displacement is applied to the top of the concrete cylinder.

The advanced fundamental concrete (AFC) model (Adley et al. 2010; Nordendale et al. 2013) is chosen to describe plasticity and damage behavior in the homogenized continuum in this simulation. In this paper, we use the plastic strain evolution in the AFC model (see Appendix for detailed yield function). Further, instead of using the empirical damage evolution in the AFC model, we extract the damage evolution functions obtained from the micro-cell simulations in Sect. 5.3 to describe the effects of microstructure randomness. The adopted material parameters for the AFC model are given in Appendix.

The tensile and shear damage evolution curves with the mean values, mean plus STD and mean minus STD are plotted in Fig. 21. Figure 22 shows the comparison between the simulation results and the test results of the confined concrete cylinder under compression. Three curves are shown in Fig. 22: the mean value of the principal stress difference, and the mean plus and minus the STD.

Due to the limited number of experimental samples, the probability distribution of the confined stress–strain relationship is unavailable. However, it is shown that the simulation results considering stochastic microstructural variations are in good agreement with the measured experimental stress–strain curves.

6 Conclusion

The stochastic description of concrete and its inherent multi-scale behavior have not yet been comprehensively understood. In this paper, we investigate the propagation of the statistical variation of concrete from

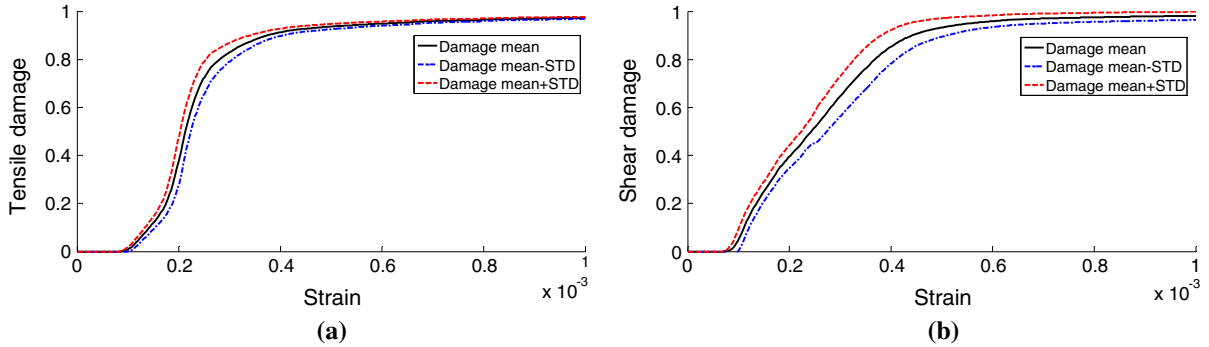

Fig. 21 Damage evolution curves used in the simulation. **a** Tensile damage, **b** shear damage

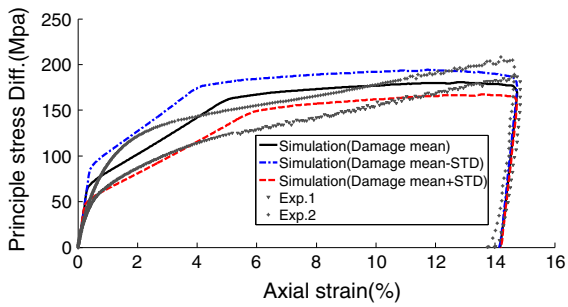

Fig. 22 Comparison of numerical results with experimental data

the micro-scale to the macro-scale by using numerical simulations and stochastic generalized density evolution method. The stochastic micro-structure of concrete is first obtained from the CT scans, by which the corresponding probability distribution of the micro-voids are obtained to describe the randomness in the micro-cell. The multi-scale free energy bridging method is introduced to obtain the homogenized stress–strain and macro-scale damage evolution functions from the micro-scale simulations of crack propagations in the micro-structures. The simulations are performed to obtain the homogenized stress–strain curves, HFE histories, and the damage evolution functions. Finally, the generalized density evolution equation is introduced to obtain the probability description of damage evolution functions.

This study shows, while with the lognormal micro-voids dimensions and uniform micro-voids distributions are used as input, the resulting PDFs of the macroscopic damage evolution functions can be quite irregular.

In this work, the COV between different scales is defined to quantify the probability variation between scales. Numerical investigation demonstrates that the statistical variations in macro-scale damage state are smaller than the statistical variations in the voids dimensions in the microstructures. The simulation results further show that the COV in shear damage is larger than the one in the tensile damage even for the same micro-cell geometries with identical material parameters. This observation suggests that different fracture processes under different loading conditions play an important role in randomness transmission to larger scales. The effectiveness of the proposed method is validated through the triaxial compression of concrete specimens, and good agreement between experimental and computational results is observed.

Acknowledgements The support of this work by US Army Engineer Research and Development Center under contract W912HZ-07-C-0019 to the second, fourth, fifth, sixth and seventh authors, and National Science Foundation of China under Grant No. U1134209 and Grant No. 91315301 to Tongji University for the third author is gratefully acknowledged.

Appendix

As discussed in Sect. 2, the damage evolution functions are extracted from the micro-cell simulation using energy bridging. These damage evolution functions are used in the elastic damage model of concrete. The plastic behavior of concrete under compression (Ortiz 1985; Faria et al. 1998; Lee and Fenves 1998) is also considered in this work. Under the continuum damage mechanics framework (Faria et al. 1998; Wu et al. 2006), the total HFE $\bar{\psi}^m$ can be expressed as the sum

of the elastic HFE $\bar{\psi}^e$ from the micro-cell simulation and plastic HFE.

$$\bar{\psi}^m = \bar{\psi}^e + \bar{\psi}^p \tag{49}$$

In Eq. (49), the elastic HFE can be expressed as

$$\bar{\psi}^e = \frac{1}{2}\bar{\boldsymbol{\sigma}} : \bar{\boldsymbol{\varepsilon}}^e \tag{50}$$

where $\bar{\boldsymbol{\varepsilon}}^e = \bar{\boldsymbol{\varepsilon}} - \bar{\boldsymbol{\varepsilon}}^p$. A decomposition of the effective stress is given as

$$\bar{\boldsymbol{\sigma}} = \boldsymbol{C}_0 : \left(\bar{\boldsymbol{\varepsilon}} - \bar{\boldsymbol{\varepsilon}}^P\right) = \boldsymbol{C}_0 : \bar{\boldsymbol{\varepsilon}}^e = \bar{\boldsymbol{\sigma}}^{vol} + \bar{\boldsymbol{\sigma}}^{dev} \tag{51}$$

where $\bar{\boldsymbol{\sigma}}^{vol}$ and $\bar{\boldsymbol{\sigma}}^{dev}$ are the effective deviatoric and volumetric stresses, respectively. Comparing Eqs. (50) with (20), $\bar{\psi}^e$ can be replaced by $\bar{\psi}$ ($\bar{\psi}^e = \bar{\psi}$) when the elastic micro-cell analysis is performed ($\bar{\boldsymbol{\varepsilon}} = \bar{\boldsymbol{\varepsilon}}^e$). According to the experimental results (Ortiz 1985; Faria et al. 1998; Lee and Fenves 1998), concrete shows little, almost no plastic strain under tension. Therefore, Eq. (49) can be rewrite as

$$\begin{aligned}\bar{\psi}^m\left(\bar{\varepsilon}^e, \bar{\varepsilon}^p, \boldsymbol{\kappa}, d^t, d^s\right) &= \bar{\psi}^e\left(\bar{\varepsilon}^e, d^t, d^s\right) \\ &+ \bar{\psi}^p\left(\bar{\varepsilon}^e, \bar{\varepsilon}^p, \boldsymbol{\kappa}, d^s\right)\end{aligned} \tag{52}$$

where $\boldsymbol{\kappa}$ denotes a suitable set of plastic variables, and d^t and d^s are tensile and shear damage parameters, respectively.

The elastic and plastic HFE's are defined as

$$\begin{aligned}\bar{\psi}^e\left(\bar{\boldsymbol{\varepsilon}}^e, d^t, d^s\right) = \int_0^{\bar{\varepsilon}^e} &\Big[\left(1-d^t\right)\bar{\boldsymbol{\sigma}}^{vol} \\ &+ \left(1-d^s\right)\bar{\boldsymbol{\sigma}}^{dev}\Big] : d\bar{\boldsymbol{\varepsilon}}^e\end{aligned} \tag{53}$$

$$\bar{\psi}^p\left(\bar{\varepsilon}^e, \bar{\varepsilon}^p, \boldsymbol{\kappa}, d^s\right) = \left(1-d^s\right)\int_0^{\varepsilon^p} \bar{\boldsymbol{\varepsilon}}^e : C_0 : d\bar{\varepsilon}^p \tag{54}$$

According to the second principle of thermodynamics, any arbitrary irreversible process satisfies the (Coleman and Gurtin 1967) inequality, of which the reduced form is

$$\dot{\gamma} = -\dot{\bar{\psi}}^m + \bar{\boldsymbol{\sigma}} : \dot{\bar{\boldsymbol{\varepsilon}}} \geq 0 \tag{55}$$

Referring to the standard thermodynamics arguments by Coleman and Gurtin (1967) and the assumption that damage and plastic unloading are elastic processes, the following conditions are satisfied for any admissible process as:

$$\bar{\boldsymbol{\sigma}} = \frac{\bar{\psi}^e}{\partial \bar{\boldsymbol{\varepsilon}}^e} \tag{56}$$

$$\dot{\gamma}^d = \left(\frac{\partial \bar{\psi}^m}{\partial d^t}\dot{d}^t + \frac{\partial \bar{\psi}^m}{\partial d^s}\dot{d}^s\right) \geq 0 \tag{57}$$

$$\dot{\gamma}^p = \left(\bar{\boldsymbol{\sigma}} : \dot{\bar{\boldsymbol{\varepsilon}}}^p + \frac{\partial \bar{\psi}^m}{\partial \boldsymbol{\kappa}}\dot{\boldsymbol{\kappa}}\right) \geq 0 \tag{58}$$

It can be clearly seen in Eq. (56), the homogenized stress is only dependent on the elastic HFE. Taking Eq. (56) into consideration, the damage evolution is assumed to be only associated with the elastic HFE, and the independent evolution model can be introduced for the plastic deformation. It is noted that Eqs. (57) and (58) express the irreversible damage and plastic processes. The construction of damage evolution functions follow the energy bridging procedures described in Eqs. (27) and (28).

The Advanced Fundamental Concrete (AFC) model (Adley et al. 2010) coupled with the tension and shear damage evolution functions (Lin et al. 2016) is employed in this paper as the concrete material model. In this modified AFC model, when the first invariant of the stress tensor (I_1) is less than or equal to zero, the yield surface is expressed as

$$\begin{aligned}Y_c = \left\|\bar{\boldsymbol{\sigma}}^{dev}\right\| - &\Big(C_1 - \left(C_2 + (C_1 - C_2)\, d^s\right) e^{A_n I_1} \\ &- C_4 I_1\Big)\left(1 + C_3 \ln(\dot{\bar{\varepsilon}}_n^{dev})\right)\end{aligned} \tag{59}$$

where C_1, C_2, C_3, C_4 and A_n are the parameters related to the initial yield surface and confinement state, $\dot{\bar{\varepsilon}}_n^{dev} = \frac{\dot{\bar{\varepsilon}}}{\bar{\varepsilon}_0^t}$ is the effective deviatoric strain rate (Shkolnik 2008) normalized by a reference strain rate $\bar{\varepsilon}_0^t$. Based on the assumption in AFC model (Adley et al. 2010), the value of $(C_1 - C_2)$ represents the initial yield point.

To capture the hardening of the concrete under compression, we modify the parameter C_1 as

$$C_1 = C_1^*(1 + h\bar{\varepsilon}^p) \tag{60}$$

$$h = \begin{cases} h_a & \left\|\bar{\boldsymbol{\sigma}}^{dev}\right\| \leq \sigma_d \\ h_b & \left\|\bar{\boldsymbol{\sigma}}^{dev}\right\| \geq \sigma_d \end{cases} \tag{61}$$

where σ_d is the damage initiation stress which is assumed to be a function of the first invariant of the stress tensor (I_1):

$$\sigma_d = a_1 + a_2 I_1 + a_3 I_1^2 \tag{62}$$

Table 1 Material parameters in the simulation

Variable	Description	Value
E	Young's modulus	$E = 24500$ MPa
v	Poisson's ratio	$v = 0.16$
ρ	Density of the concrete	2400 Kg/m^3
C_1^*	Yield surface constants	98.25MPa
C_2		55 MPa
C_3		0.0125
C_4		0.002433
A_n		5.78×10^{-10} Pa^{-1}
h_a	Hardening constants	11
h_b		0.2
$\bar{\varepsilon}_0^t$	Reference strain rate	0.00034s^{-1}
a_1	Damage initiation parameters	0.375×10^8
a_2		-0.1958
a_3		-0.049×10^8

According to the "effective stress space plasticity" (Faria et al. 1998; Wu et al. 2006), the evolution law of plastic strain is expressed as follows:

$$\dot{\bar{\boldsymbol{\varepsilon}}}^p = \dot{\lambda}^p \frac{\partial Y_c}{\partial \bar{\boldsymbol{\sigma}}} \tag{63}$$

where $\dot{\bar{\boldsymbol{\varepsilon}}}^p$ is the plastic strain rate and $\dot{\lambda}^p$ is the plastic flow consistency parameter.

The plasticity parameters for the AFC model employed in this work are listed in Table. 1.

References

Adley M, Frank A, Danielson K et al (2010) The advanced fundamental concrete (AFC) model: TR-10-X. US Army Engineer Research and Development Center, Vicksburg, MS

Bazant ZP, Caner FC, Carol I et al (2000) Microplane model M4 for concrete. I: formulation with work-conjugate deviatoric stress. J Eng Mech 126(9):944–953

Bazant ZP, Planas J (1998) Fracture and size effect in concrete and other quasibrittle materials. CRC Press, Boca Raton

Chen JS, Pan CH, Wu CT et al (1996) Reproducing kernel particle methods for large deformation analysis of non-linear structures. Comput Methods Appl Mech Eng 139(1):195–227

Chen JB, Li J (2009) A note on the principle of preservation of probability and probability density evolution equation. Probab Eng Mech 24(1):51–59

Coleman BD, Gurtin ME (1967) Thermodynamics with internal state variables. J Chem Phys 47(2):597–613

Dascalu C, Bilbie G, Agiasofitou EK (2008) Damage and size effects in elastic solids: a homogenization approach. Int J Solids Struct 45(2):409–430

Döbert C, Mahnken R, Stein E (2000) Numerical simulation of interface debonding with a combined damage/friction constitutive model. Comput Mech 25(5):456–467

Faria R, Oliver J, Cervera M (1998) A strain-based plastic viscous-damage model for massive concrete structures. Int J Solids Struct 35(14):1533–1558

Fish J, Yu Q, Shek K (1999) Computational damage mechanics for composite materials based on mathematical homogenization. Int J Numer Methods Eng 45(11):1657–1679

Gibbs JW (2010) Elementary principles in statistical mechanics: developed with especial reference to the rational foundation of thermodynamics. Cambridge University Press, Cambridge

Heard WF (2014) Development and multi-scale characterization of a self-consolidating high-strength concrete for quasi-static and transient loads. Vanderbilt University, Nashville

Hill R (1984) On macroscopic effects of heterogeneity in elastoplastic media at finite strain. Math Proc Camb Philos Soc 95:481–494

Huet C (1990) Application of variational concepts to size effects in elastic heterogeneous bodies. J Mech Phys Solids 38(6):813–841

Huet C (1991) Hierarchies and bounds for size effects in heterogeneous bodies. Models Discret Syst 2:127–134

Kamiński M (2007) Generalized perturbation-based stochastic finite element method in elastostatics. Comput Struct 85(10):586–594

Kamiński M, Kleiber M (2000) Perturbation based stochastic finite element method for homogenization of two-phase elastic composites. Comput Struct 78(6):811–826

Lee J, Fenves GL (1998) Plastic-damage model for cyclic loading of concrete structures. J Eng Mech 124(8):892–900

Li J, Chen JB (2004) Probability density evolution method for dynamic response analysis of structures with uncertain parameters. Comput Mech 34(5):400–409

Li J, Chen JB (2007) The number theoretical method in response analysis of nonlinear stochastic structures. Comput Mech 39(6):693–708

Li J, Chen JB (2008) The principle of preservation of probability and the generalized density evolution equation. Struct Saf 30(1):65–77

Lin SP, Chen JS, Liang SX (2016) A damage analysis for brittle materials using stochastic micro-structural information. Comput Mech 57(3):371–385

Li J, Ren X (2011) Multi-scale based stochastic damage evolution. Eng Fail Anal 18(2):726–734

Liu WK, Jun S, Zhang YF (1995) Reproducing kernel particle methods. Int J Numer Methods Fluids 20(8–9):1081–1106

Moës N, Belytschko T (2002) Extended finite element method for cohesive crack growth. Eng Fract Mech 69(7):813–833

Moës N, Dolbow J, Belytschko T (1999) A finite element method for crack growth without remeshing. Int J Numer Methods Eng 46(1):131–150

Nordendale NA, Heard WF, Hickman MA et al (2013) Cementitious material models for simulating projectile impact effects. Comput Mater Sci 79:745–758

Ortiz M (1985) A constitutive theory for the inelastic behavior of concrete. Mech Mater 4(1):67–93

Ostoja-Starzewski M (2001) Microstructural randomness versus representative volume element in thermomechanics. J Appl Mech 69(1):25–35

Ostoja-Starzewski M (2006) Material spatial randomness: from statistical to representative volume element. Probab Eng Mech 2:112–132

Ren X, Chen JS, Li J et al (2011) Micro-cracks informed damage models for brittle solids. Int J Solids Struct 48(10):1560–1571

Sakata S, Ashida F, Kojima T (2008) Stochastic homogenization analysis on elastic properties of fiber reinforced composites using the equivalent inclusion method and perturbation method. Int J Solids Struct 45(25):6553–6565

Shah SP (1995) Fracture mechanics of concrete: applications of fracture mechanics to concrete, rock and other quasi-brittle materials. Wiley, London

Shkolnik IE (2008) Influence of high strain rates on stress-strain relationship, strength and elastic modulus of concrete. Cem Concr Compos 30(10):1000–1012

Tootkaboni M, Graham Brady L (2010) A multi-scale spectral stochastic method for homogenization of multi-phase periodic composites with random material properties. Int J Numer Methods Eng 83(1):59–90

Wu JY, Li J, Faria R (2006) An energy release rate-based plastic-damage model for concrete. Int J Solids Struct 43(3):583–612

Xu XF (2007) A multiscale stochastic finite element method on elliptic problems involving uncertainties. Comput Methods Appl Mech Eng 196(25):2723–2736

Xu J, Chen JB, Li J (2012) Probability density evolution analysis of engineering structures via cubature points. Comput Mech 50(1):135–156

Xu XF, Graham-Brady L (2006) Computational stochastic homogenization of random media elliptic problems using Fourier Galerkin method. Finite Elements Anal Design 42(7):613–622